International Journal of Thermophysics, Vol. 22, No. 2, 2001

Thermophysical Properties of Fluids from Dynamic Light Scattering[1]

S. Will[2–4] and A. Leipertz[2]

In a continuous development for more than three decades, dynamic light scattering (DLS) has evolved into a versatile and powerful technique for the determination of transport and other thermophysical properties of fluids. The success is founded on its application in a macroscopic thermodynamic equilibrium, i.e., without the need for employing external gradients, to determine a large variety of properties, which can be derived, in some instances even simultaneously, by an appropriate experimental approach and a corresponding signal analysis. The principles, essential features, and variants of the technique are reviewed, and a survey on the determination of various desired transport and thermophysical properties is given, both for the application of light scattering from bulk fluids and for the variant of surface light scattering (SLS). The stage of development and the corresponding uncertainties are discussed for the measurement of the individual quantities, and the performance of the method is demonstrated by representative experimental results for relevant fluids.

KEY WORDS: dynamic light scattering; surface light scattering; thermophysical properties; transport coefficients.

1. INTRODUCTION

The exact experimental determination of properties of fluids is a central research task in the field of thermophysics, as various thermophysical data are closely related with the setup and verification of equations of state. A reliable knowledge of thermophysical data is also essential for an optimized

[1] Invited paper presented at the Fourteenth Symposium on Thermophysical Properties, June 25–30, 2000, Boulder, Colorado, U.S.A.

[2] Lehrstuhl für Technische Thermodynamik (LTT), Friedrich-Alexander-Universität Erlangen-Nürnberg, Am Weichselgarten 8, D-91058 Erlangen, Germany.

[3] Technische Thermodynamik/Wärme- und Stofftransport (TTWSt), Universität Bremen, FB4, Badgasteiner Straße 1, D-28359 Bremen, Germany.

[4] To whom correspondence should be addressed. E-mail: sw@ltt.uni-erlangen.de

0195-928X/01/0300-0317$19.50/0

design of processes and apparatus in various engineering disciplines, and, in particular, the provision of accurate values for the coefficients of heat, mass, and momentum transfer is required [1]. This necessity is partly reflected in the continuous development and improvement of various experimental methods for the determination of transport coefficients [2]. In parallel to nonoptical methods, light scattering techniques have evolved, constantly been improved, and found increasing practical application. Their success is based mainly on two facts, namely, the possibilities to apply them in (or for some techniques close to) thermodynamic equilibrium and to obtain various properties with one single basic approach and setup, and in some instances even simultaneously.

Dynamic light scattering (DLS) probes statistical fluctuations inherent in all fluid systems. In bulk fluids, these are microscopic changes in temperature, pressure, and/or concentration which result in variations of the dielectric constant ε (and the refractive index n). With conventional techniques for the measurement of transport properties, external gradients are required, large enough to induce a reasonably measurable flux of energy, momentum, or mass according to the respective gradient and small enough to render the system properties only slightly affected. In contrast, DLS makes use of quasi-self-induced gradients with the minimum amplitude possible, and it is the decay of these statistical perturbations which is monitored by the scattered light signal. A central element of this concept is Onsager's regression hypothesis [3], which states that the decay of these microscopic fluctuations is subject to the same transport properties that it is for macroscopic transport phenomena.

Besides the transport and thermophysical data to be obtained from light scattering from the bulk fluid—which are detailed in the next section—also the interaction of light with fluctuations at the surface of a fluid or, more generally, at the interface between the fluids may be utilized to yield information on the thermophysical properties of the fluids which control the decay of these thermally excited interface fluctuations. The evaluation of the corresponding signal from surface light scattering (SLS) yields information on viscosity and surface tension.

This paper presents an overview of the current state of the DLS technique, including its variant SLS, for the determination of thermophysical properties of fluids. After a brief review on the basic aspects of DLS (for a more comprehensive review on the physical foundations, see, e.g., Berne and Pecora [4] and Chu [5]), the light scattering experiment is given a more detailed treatment, which, in particular, includes aspects of experiment design, data evaluation, and error analysis. The important role of DLS for the determination of thermophysical properties is demonstrated by various application examples, with a focus on various chlorine-free

refrigerants, a substance class, where DLS has amply contributed to the provision of required data, and toluene, both an important intermediate in chemical industry and a test fluid for experimental methods with a wide liquid range of 178 to 594 K.

The present paper may in some aspects be regarded as an update of former reviews on light scattering techniques [7–10]. It is restricted to light scattering from spontaneous fluctuations. For a description of the forced Rayleigh scattering (or laser-induced thermal grating) technique, a related method, which makes use of deliberately induced small gradients in various variants, the reader is referred to the specialized literature [11–15].

2. PRINCIPLES OF DYNAMIC LIGHT SCATTERING

2.1. Scattered Light Spectra

When a fluid sample in thermodynamic equilibrium is irradiated with coherent light, the scattered light exhibits a characteristic spectrum, which is determined by the scattering geometry and the individual thermophysical properties. The first enters through the scattering vector $\vec{q} := \vec{k}_i - \vec{k}_s$, where $\vec{k}_i$ and $\vec{k}_s$ denote the wave vectors of the incident and scattered light, respectively. For the quasi-elastic scattering process, i.e., for $k_s \cong k_i$, the modulus of the scattering vector directly follows from the geometry (Fig. 1)

$$q = |\vec{k}_i - \vec{k}_s| \cong 2k_i \sin(\Theta/2) = \frac{4\pi n}{\lambda_0} \sin(\Theta/2) \tag{1}$$

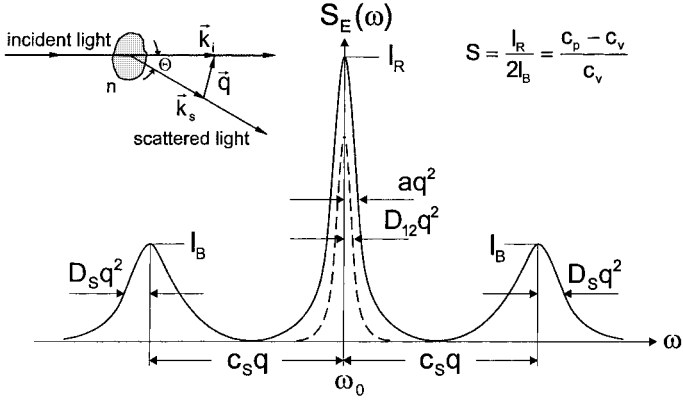

Fig. 1. Basic scheme of the scattering process and the spectrum obtained from a bulk fluid. The Landau–Placzek ratio S is given by the amplitudes of the Rayleigh and Brillouin lines, respectively.

where n is the refractive index of the fluid, λ_0 is the light wavelength in vacuo, and Θ is the scattering angle.

Figure 1 schematically shows how the various desired properties are quasi-encoded in the spectrum (for a comprehensive and rigorous treatment of scattered light spectra, see Berne and Pecora [4] and Mountain [16]). The central Rayleigh line exhibits a pure Lorentzian shape only in the case of a pure and simple fluid. For fluid mixtures it becomes a superposition of the contributions from temperature and concentration fluctuations, with the individual half-widths characterized by the respective transport properties. Whether one succeeds in the experimental recovery of the desired properties depends mainly on the intensity of these contributions, as governed by the difference of the refractive indices of the compounds and the difference between the linewidths. When adding seed particles to a fluid or mixture, the central part of the spectrum is normally governed by the contribution of the particle diffusion with a characteristic coefficient D_p, which, through the Stokes–Einstein equation [17],

$$D_p = kT/(6\pi\eta r) \tag{2}$$

is connected with the particle radius r and dynamic viscosity η. Applied to a fluid mixture, with a favorable relation between the intensity and the linewidths of the contributions, a simultaneous determination of them is basically feasible.

In contrast to the Rayleigh line, the two Brillouin (or Brillouin–Mandel'shtam) lines exhibit a (practically symmetric) frequency shift, which follows from the ultrasonic velocity c_s and the modulus of the scattering vector. Although these lines basically exhibit a Lorentzian shape, too, the relation of an experimentally determined linewidth, which is typically several orders of magnitude larger than those of the Rayleigh line (cf. Table I), to sound attenuation poses some difficulty. With all conventional light scattering setups the scattering vector exhibits some fundamental uncertainty, i.e., due to a finite aperture of the detection system, light from a range of scattering vectors with a modulus in an interval $[q-\delta q; q+\delta q]$ will contribute to the detected signal. As δq is usually many orders of magnitude smaller than q, this fundamental lack of definition has a completely negligible effect on the determination of transport properties from the Rayleigh line. With the typically large frequency spacing of the Brillouin lines, however, a small lack of definition in the scattering vector results in some uncertainty, or smearing, in the position of the Brillouin lines, which may have an order of magnitude comparable to that of the linewidths themselves [18–20]. The recovery of the original linewidth, and thus of the sound attenuation, basically requires a deconvolution of the

Table I. Characteristic Linewidths $\Gamma(=1/\tau_c)$ and Frequency Spacings ($\Delta\omega$) for Simple Liquids such as Toluene under Ambient Conditions[a]

θ_i (deg)	q (m^{-1})	$\Delta\omega_B$ (rad·s^{-1})	Γ_B (rad·s^{-1})	Γ_t (rad·s^{-1})	Γ_{12} (rad·s^{-1})	Γ_p (rad·s^{-1})	$\Delta\omega_s$ (rad·s^{-1})	Γ_s (rad·s^{-1})
2	4.5×10^5	6.0×10^8	1.6×10^6	1.8×10^4	3.7×10^2	0.74	1.7×10^6	2.7×10^5
5	1.1×10^6	1.5×10^9	1.0×10^7	1.1×10^5	2.3×10^3	4.6	6.8×10^6	1.7×10^6
20	4.4×10^6	5.9×10^9	1.6×10^8	1.7×10^6	3.5×10^4	71	5.3×10^7	2.6×10^7
90	2.7×10^7	3.6×10^{10}	6.0×10^9	6.7×10^7	1.4×10^6	2.8×10^3	—	—

[a] The subscripts denote Brillouin components (B), the respective modes of thermal (t), mutual (12), and particle (p) diffusion for the Rayleigh line, and the quantities in surface light scattering (s). The values for the scattering vector q are based on a laser wavelength of 488 nm and a rectangular cross section of the sample cell.

experimentally obtained spectrum or other models to take this effect into account.

In a similar way to light scattering from bulk fluids in "classical" DLS, the variant of surface light scattering probes natural fluctuations without employing external gradients. In this case, the decay of thermally excited waves, quantized in so-called "ripplons" [21], on liquid surfaces or—more generally and more precisely—interfaces between a liquid and, usually, a vapor phase is investigated. Such an interface can be represented by a superposition of surface modes with different amplitudes ξ_q and wave vectors $\vec{q}$, where amplitudes are typically of the order of nanometers and wavelengths of interest are in a range of about 1 to 100 μm [22–26]. For a particular surface mode with frequency α, the time-dependent vertical displacement ξ of the surface to its flat equilibrium state at a given point $\vec{r}$ is given by

$$\xi(\vec{r}, t) = \xi_q \exp[\, i(\vec{q}\vec{r} + \alpha t)\,] \tag{3}$$

The description of individual surface modes, i.e., their dispersion relation, follows from the solution of the Navier–Stokes equation for an incompressible fluid [24, 27, 28]. For wavelengths shorter than a critical wavelength [22, 24]

$$\Lambda_c = 1.16\pi\eta^2/(\sigma\rho) \tag{4}$$

with dynamic viscosity η, surface tension σ, and density ρ, surface waves are overdamped. As an example, this critical value is about 50 nm for water at ambient conditions, and correspondingly larger for other simple liquids, as they exhibit a smaller surface tension. In most SLS experiments surface modes with longer wavelengths are observed; in this case of propagating

capillary waves the complex frequency α of a certain surface mode with frequency ω and damping Γ can be represented in a first-order approximation by

$$\alpha = \omega + i\Gamma \approx \left[\frac{\sigma q^3}{\rho}\right]^{1/2} + i2q^2 v \tag{5}$$

where v is the kinematic viscosity. Two points are important to note in this context: First, the succinct but approximate solution of Eq. (5) does not normally suffice to provide values on surface tension and viscosity with the desired accuracy. Rather, it is necessary to solve the full dispersion relation either numerically or to a higher order [25, 28]. Second, the formulation of Eq. (5) completely ignores the presence of a vapor phase and relates all properties solely to the liquid phase. Taking the vapor phase into account, Eq. (5) must be modified according to

$$\alpha = \omega + i\Gamma \approx \left[\frac{\sigma q^3}{\rho' + \rho''}\right]^{1/2} + i2q^2 \frac{\eta' + \eta''}{\rho' + \rho''} \tag{6}$$

where ρ' and ρ'' are the densities and η' and η'' are the dynamic viscosities of the liquid and vapor phases, respectively. It is obvious that Eq. (5) is a reasonable approximation if both the density and the viscosity of the vapor phase are low compared to the respective liquid values, e.g., if measurements on a pure fluid are performed for moderate vapor pressures, or if the respective values are similar, i.e., in the vicinity of the critical point. More specifically, the maximum error introduced by this neglect under unfavorable conditions remains below 5% for various refrigerants [29]. As the vapor properties may be treated like a correction in many practical instances, even the provision of approximate or estimated values for ρ'' and η'' ensures the required accuracy of surface tension and liquid viscosity.

Similarly to the spectrum of light scattered from a bulk fluid, the SLS spectrum in most cases of interest exhibits two frequency-shifted lines, this time from propagating surface waves, in contrast to propagating sound waves in the former case. Another difference important for signal acquisition and evaluation is that the frequency shift is typically two orders of magnitude smaller, resulting in only negligible line broadening due to the lack of definition in the scattering vector if not too small scattering angles are chosen (see Section 3.2). The Lorentzian shape of these lines, as well as the approximate relations for v and σ as given in Fig. 2, hold only in the limiting case of a high ratio $y = \sigma\rho/(4\eta^2 q)$, where $y = 0.145$ corresponds to the critical wavelength of Eq. (4). In approaching this value, the lineshapes become more complex [25, 30], and in the case of small y, overdamped waves with a single central Lorentzian are obtained.

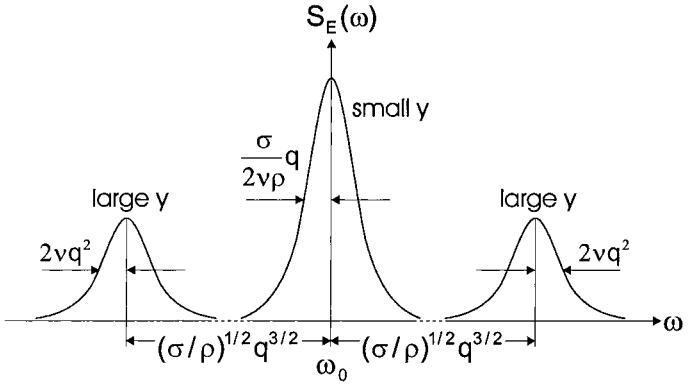

Fig. 2. Unifying and approximate representation of possible SLS spectra: depending on the fluid and setup characteristics, either propagating or overdamped capillary waves are observed, which result in frequency-shifted or just broadened spectral lines, respectively.

2.2. Correlation Technique

The straightforward way to obtain the desired properties would be a measurement of the intensity spectrum of scattered light. The linewidths of the order of megahertz and below, encountered in typical light scattering experiments (cf. Table I), are so small compared to the frequency of light (order of 6×10^{14} Hz) that they are clearly below the resolving power of direct instruments, such as Fabry–Perot interferometers, and direct observation is possible only in Brillouin investigations at large angles [18, 31].

While a spectral approach becomes possible only using heterodyne techniques (see next subsection), a convenient method of analysis can be performed in the time domain. According to the Wiener–Khintchine theorem, the power-spectral density $S_E(\omega)$ is the Fourier transform of the autocorrelation function (ACF) of the electric field,

$$G^{(1)}(\tau) = \langle E_s^*(t)\, E_s(t+\tau) \rangle \tag{7}$$

where the brackets indicate the time average and the asterisk denotes the complex conjugate variable. The autocorrelation function of a variable quantifies the time scales on which changes take place in this property, and as the scattered light is modulated by the various processes in the fluid, conclusions on the underlying transport and thermophysical properties may be drawn. Through the Fourier transform the position of the spectral lines does not play a role any more, and the individual Lorentzian lines are transformed into simply exponentially decaying functions in the time

domain, each exhibiting a characteristic decay time τ_c. Thus, even in the case of light scattering from a pure fluid, the ACF exhibits two contributions, namely, from the Rayleigh and the Brillouin lines. Yet the time scales of these decays are clearly different, and the individual contributions may be easily separated. Due to differences in time scales and/or signal levels, this separation is also possible for many other practical situations, even if spectra become more complicated.

As the quantity measured by a detector is more directly related to the intensity $I_s \propto E_s^* E_s$, the intensity correlation function $G^{(2)}(\tau)$ is usually the observable of interest. Normalized to its value for $\tau = \infty$, the idealized correlation function for a single diffusive process takes the form $g^{(2)}(\tau) = 1 + \exp(-2\tau/\tau_c)$, where $\tau_c = 1/(Dq^2)$ is the decay time of the field correlation function and the diffusion constant D may—depending on the process investigated—be identified with the thermal diffusivity a, the mutual diffusion coefficient D_{12}, or the particle diffusion coefficient D_p. In practical cases, two modifications have to be taken into account. First, slow fluctuations, mostly at time scales quite different from those of interest, will result in slight deviations of the baseline from unity. Second, as—in particular—spatial coherence will not be perfect, the amplitude of the decay will not be unity, but somewhat lower. These corrections are practically taken as fit parameters resulting in a working equation of the DLS instrument of the form,

$$g^{(2)}(\tau) = a + b \exp(-2\tau/\tau_c) \tag{8}$$

2.3. Homodyne and Heterodyne Techniques

In practice, there may be not only light from the scattering process itself impinging onto the detector, but also coherent contributions of stray light. In this case, a more general form of the correlation function is

$$G^{(2)}(\tau) = (I_0 + I_s)^2 + I_s^2 e^{-2\tau/\tau_c} + 2I_0 I_s e^{-\tau/\tau_c} \tag{9}$$

where I_0 is the additional signal from the so-called "local oscillator."

As the accuracy in determining the decay time from an equation of this form is clearly worse than in the case of Eq. (8), it must be the aim of the experimenter to realize conditions where one of the two exponentials in Eq. (9) clearly dominates. Homodyne conditions prevail when the scattered light signal is comparatively strong. For determination of the thermal diffusivity and the mutual diffusion coefficient, the condition $I_s \gg I_0$ can excellently be fulfilled in the vicinity of critical points [32, 33]. Homodyne conditions can also easily be maintained in the case of particle scattering

for the measurement of viscosity [34, 35]. In the case of SLS a reasonable homodyne experiment can be realized only for ultralow surface tensions or, again, close to critical points [24]. In all other cases it is advisable to realize defined heterodyne conditions, $I_0 \gg I_s$, by provision of a local-oscillator, e.g., through imaging part of the incident light directly onto the detector. A heterodyne approach is also used in the investigation of the Brillouin components of the spectrum. To this end, the frequency of the local oscillator is shifted, e.g., by an acoustooptic modulator, in order nearly to match the frequency of one of the Brillouin components. Thus, the signal can be strongly enhanced compared to the Rayleigh line, and the residual frequency difference $\Delta\omega = |\omega_B - \omega_0|$ between the Brillouin line (index B) and the reference signal can easily be resolved experimentally. The correlation function now reads

$$G^{(2)}(\tau) = A + Be^{-\tau/\tau_c} \cos(\Delta\omega\tau) \tag{10}$$

In a similar way, the correlation function is obtained in the case of propagating waves for SLS. As the spacing to the frequency of the incident light is typically at least one order of magnitude smaller than in the case above, a deliberate frequency shift is not necessary in this instance.

3. LIGHT SCATTERING EXPERIMENT

3.1. General Instrument Design

The range of possible setups for DLS experiments is very wide, and naturally the exact choice of components depends on the specific application. Design details and variants may be found in the literature [5, 36, 37], yet the setup sketched in Fig. 3 may be regarded as a suitable basis for a variety of investigations.

Continuous-wave lasers used for DLS comprise low-power HeNe or semiconductor lasers, which suffice, e.g., for investigations close to critical points or measuring particle diffusion, and argon or solid-state lasers (e.g., $Nd:YVO_4$) with output powers of several hundred milliwatts, which are employed for measurements of thermal diffusivity, in particular, in the gas phase far from the critical point. In any case lasers are normally used with a linear polarization perpendicular to the scattering plane, and—in heterodyne experiments—they must exhibit a coherence length larger than possible path differences.

In order to provide a large signal or, more concisely, a good signal-to-noise ratio, the laser beam should be focused [37, 38]. This requirement reaches a limit if—in connection with the laser power used—irradiances

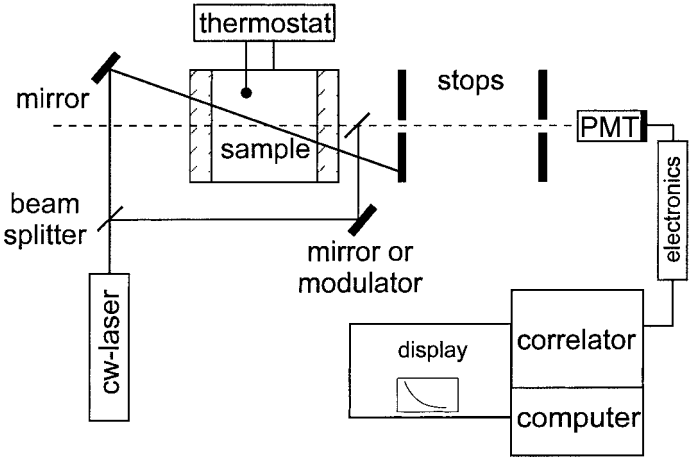

Fig. 3. Basic setup for a DLS experiment.

become too large and the sample heats up, but also through the introduction of an additional spread in the q-vector, relevant for investigations of frequency-shifted components of the spectrum.

The main criteria for the choice of the sample cell are the desired scattering angle and scattering vector for a proper investigation of the process (see also Table I). With comparatively slow processes such as mass diffusion close to the critical consolute point or particle diffusion, comparatively large scattering angles ranging up to a back-scattering geometry are used. In these cases sample cells with a cylindrical cross section are often employed, which allow easy access for all angles of incidence. Alternatively, cells with rectangular cross sections can be used, favorably in a symmetrical arrangement, in which the knowledge of the refractive index of the sample is not needed for the determination of the scattering vector [38]. With fast processes, which are relevant in connection with Brillouin scattering and the measurement of thermal diffusivity, small scattering angles, typically 3 to 5°, are used [39]. Also in this range, knowledge of the refractive index of the sample is unnecessary if one uses a very good approximation relying only on the measurement of the angle of incidence. For an exact determination of thermophysical properties the definition and measurement of the relevant thermodynamic state is essential. An important part thereof is the temperature control of the sample, which can most easily be performed through an external fluid thermostat. For higher temperatures and/or stability requirements, electrical resistance heating is normally employed, which, in connection with a passive multistage thermostat, allows a temperature stability in the millikelvin range.

The central requirement in the light detection path is that for a coherent registration of scattered light, which is a prerequisite for a large contrast in the ACF [factor b in Eq. (8)] but naturally results in a trade-off with the signal amplitude. The coherence condition may most simply be fulfilled by the use of a pair of apertures at a certain distance, yet various modifications with a conventional optical system or fiber optics are possible [5], and specifically monomode fibers may be used to obtain perfect spatial coherence [40]. The standard detector for DLS is a photomultiplier tube (PMT), operated in photon-counting mode; alternatively, an avalanche-photodiode module may be used. In order to suppress afterpulses or other correlated detector noise sources (for PMTs typically on a time scale below 10 μs), two detectors in a cross-correlation scheme are favorably employed. By this approach only commonly detected pulses originating from the desired signal are registered, at the cost, however, that signal levels are reduced by a factor of two. After amplification and discrimination detector signals are normally fed to a correlator, special-purpose hardware for the on-line computation of the ACF, where two modes of operation are common practice. In one case fixed sample times are used, which offer some ease and advantage in the acquisition and evaluation of periodic signals, i.e., those from a frequency-shifted process. In the other case sample times monotonically increase with lag times τ, which make it possible to simultaneously analyze various processes taking place on vastly different time scales. Modern correlators typically offer a few hundred channels with sample times down to the nanosecond range.

The experimentally acquired ACF may now be analyzed for the quantities of interest, mainly decay times and frequencies, by standard fit algorithms. Of course, the accuracy to be obtained in this procedure depends crucially on the noise level of the ACF [6, 41, 42]. As DLS is a statistical technique, it is essential to average over a large number of independent events (where the decay time represents the average duration) in order to get a statistically significant representation of the underlying processes. Thus, in some instances, an increase in the laser power does not help to improve the quality of the measurement; this action helps only if detector noise is the dominant noise source (as it is typically for fast processes). Instead, measurement times T have to be prolonged, or alternatively the scattering angle may be changed, in order to realize shorter decay times and to increase the ratio T/τ_c, i.e., the number of independent samples taken. The overall quality of the ACF, regarding both statistics and possible deviations from the working equation, may favorably be tested by varying the range where the fit is performed. With this multifit procedure either source of error shows up in changes in the fitted parameters [42].

3.2. Modifications for SLS

Although it has been shown that SLS may be performed in complete analogy to DLS measurements from bulk fluids using an identical setup [43], some differing design features are often employed for SLS measurements.

One obvious difference is that SLS normally investigates interfaces in horizontal orientation within a sample cell with light impinging from above. Commonly, scattered light is observed near the reflected beam, i.e., also in the top direction, which eases the optical access and is of course essential for nontransparent fluids. Alternatively, for transparent fluids scattered light may be observed close to the direction of the refracted beam [28, 29], which is advantageous as to stability considerations and scattering intensities [44], as the intensity of the refracted beam is higher than that of the reflected beam. Also, hybrid reflection–transmission geometries have been proposed [45]. As, for SLS, only the projections of the wave vectors of refracted ($\vec{k}_r$) and scattered light ($\vec{k}_s$) into the surface plane determine the scattering vector $\vec{q}$, the modulus of $\vec{q}$ is now different; for observation of scattered light within the plane of incidence, and again with the assumption of elastic scattering, $k_i \cong k_s$, one obtains for a transmission geometry [28]

$$q \cong 2k_i \sin(\Theta_s/2) \cos(\Theta_r - \Theta_s/2) = \frac{4\pi n}{\lambda_0} \sin(\Theta_s/2) \cos(\Theta_r - \Theta_s/2) \tag{11}$$

The experimental setup and the computation of the scattering vector are considerably simplified if the scattered light is observed perpendicularly to the fluid interface, i.e., in a vertical direction with $\Theta_s = \Theta_r$ (Fig. 4), where

$$q = \frac{2\pi}{\lambda_0} \sin \Theta_i \tag{12}$$

Although the generation of a local oscillator may be performed completely analogously to bulk DLS measurements, the most common approach uses a diffraction grating, especially when performing experiments in the direction of reflection [24, 26, 46]. The various diffraction orders serve as local oscillators and define specific wave-vectors for the analysis of scattered light. Regarding adjustment and coherence conditions a favorable modification is not to use the grating itself as a local oscillator but to image it onto the liquid surface. Due to the usually small frequency separation of the shifted lines in the spectrum, no frequency shift of the local oscillator is commonly necessary.

SLS experiments typically use small scattering angles, about 0.1° up to a few degrees. The according range of scattering vectors reaches from an order of 10^4/m to about 10^6/m, where large q-vectors can normally be

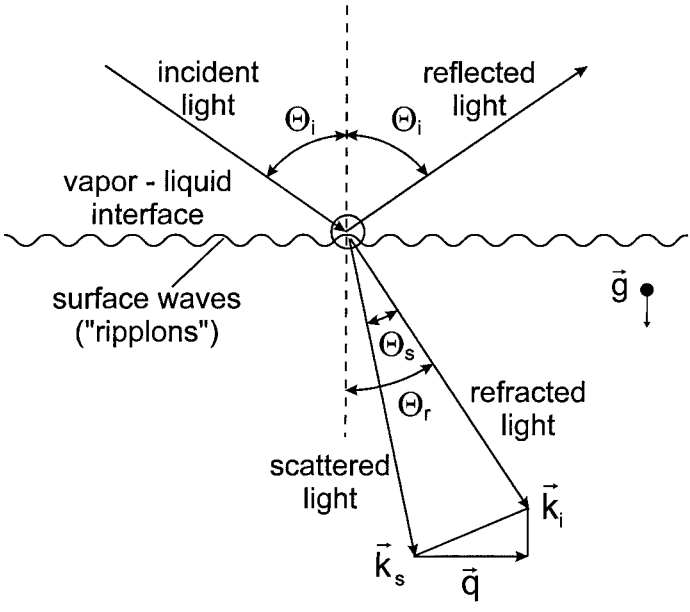

Fig. 4. Scattering geometry for an SLS experiment in transmission: favorably scattered light is detected perpendicularly to the fluid interface, i.e., with the choice $\Theta_s = \Theta_r$.

achieved only with a transmission geometry due to intensity considerations. An additional advantage of larger scattering vectors is that spectral broadening effects due to an uncertainty δq in the scattering vector do not play a role in the higher q-range, as the linewidth Γ scales with q^2, whereas $\delta\omega = [\partial(\Delta\omega)/\partial q]\,\delta q \propto q^{1/2}$ for the uncertainty $\delta\omega$ in the position of the line.

While DLS from bulk fluid relies almost exclusively on data analysis in the time domain, i.e., by photon-correlation spectroscopy (PCS), a variety of applications of SLS is found both in the time domain using a correlator and in the frequency domain using a wave analyzer, which are of course only two ways of interpretation of identical processes. The various approaches to data acquisition and analysis are discussed in detail in the literature [24, 26, 46].

4. DLS RESULTS

4.1. Thermal Diffusivity

The thermal diffusivity a is probably the transport property for which the development of DLS is most advanced [39, 47–49] and where it shows

a particular benefit, as an accurate direct determination of a is hardly possible by any other technique. Other methods measure the thermal conductivity λ, which is related to a via density ρ and isobaric heat capacity c_p: $a = \lambda/(\rho c_p)$.

The measurement of a may routinely be performed for a wide temperature range basically for both the liquid and the vapor phases, yet due to low signal levels and accordingly long measurement times, measurements are rarely performed in the gas phase far from the critical point. In contrast, with increasing signal levels, times for single experiments of a few minutes or even below may be achieved. As DLS is a statistical technique, one major source of uncertainty is the statistical accuracy with which the decay time can be obtained from the ACF. This value of course depends mainly on the noise level and thus on the patience of the experimenter, as similarly does the extent to which possible systematic deviations can be excluded [42]. A reasonable practical value for the uncertainty in the decay time is about 1%. Another major source of uncertainty is the determination of the scattering vector, which contributes about the same order of magnitude. In summary, with proper variation of the experimental parameters the resulting error may regarded to be mainly of a statistical nature [48], and a total uncertainty of about 2%—a proper definition and measurement of the thermodynamic state provided—can routinely be

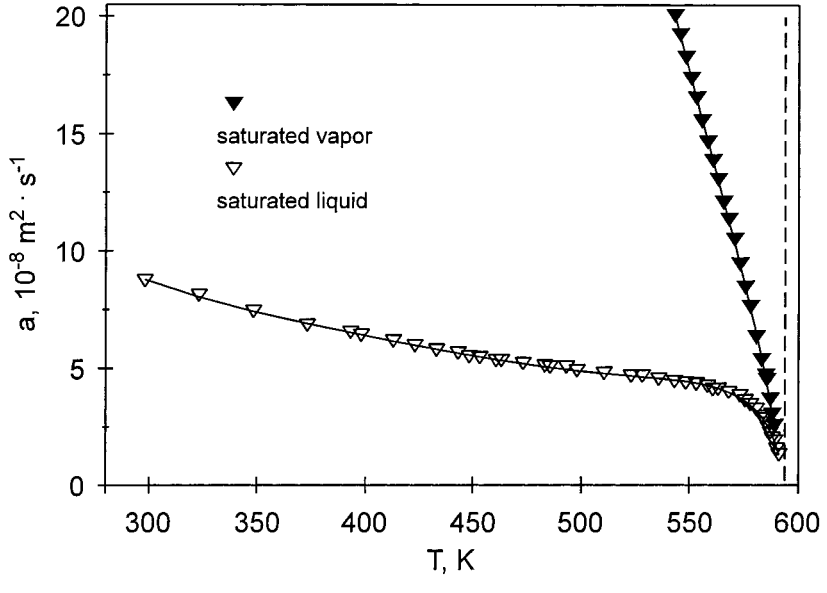

Fig. 5. Thermal diffusivity of toluene at saturation up to the critical point.

achieved for the measurement of the thermal diffusivity. The application of DLS to the determination of a is illustrated in Fig. 5, where this property has been measured for toluene up to the critical point.

The accuracy of the determination of a in fluid mixtures (beside measurement time) depends essentially on the ratio of signals from thermal diffusion to this or those from mass diffusion, the latter in turn being determined by the difference in the refractive indices of the compounds involved. If this difference is small, i.e., if the thermal diffusion signal clearly dominates the ACF, a may be measured with an accuracy similar to that in the case of a pure fluid [49, 50]. For the other extreme, if the amplitude of the thermal diffusivity signal amounts only to a few percent of that for mass diffusion, the error may rise up to several tens percent [51, 52] (see also Fig. 6).

4.2. Mutual Diffusion Coefficient

Mutual mass diffusion typically has an intermediate position between thermal and particle diffusion with regard to both signal amplitudes and

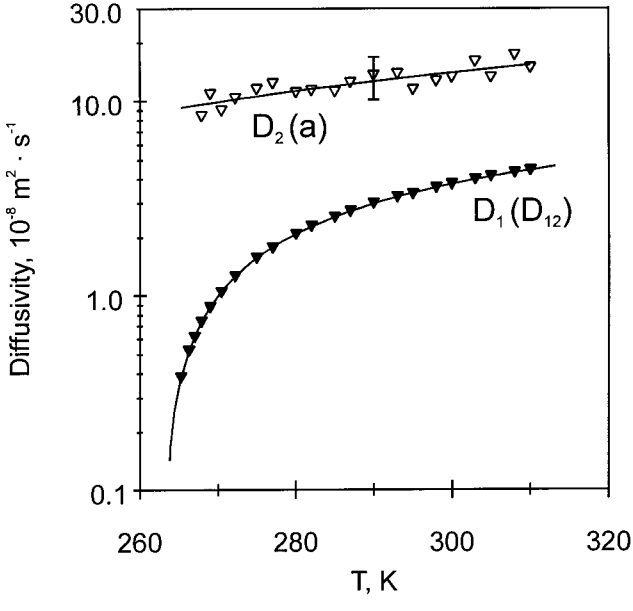

Fig. 6. Simultaneously acquired diffusion modes of an equimolar methane–ethane mixture along the critical isochore. The signal amplitude of the slow mode 1 is about 20 to 100 times higher than that of the fast mode 2.

time scales. It is therefore obvious and particularly interesting to try to perform simultaneous measurements of the mutual diffusion coefficient D_{12} together with the determination of either viscosity η [33, 34] or thermal diffusivity a [50, 52], where the setup is realized according to the respective guidelines. In the latter case small angles are employed, and the accuracy in this property again depends on the ratios of the contributions from thermal and mutual diffusivities regarding signal levels and decay times.

Basically there is always a signal from thermal diffusion present in the ACF, yet if the mass diffusion signal dominates or, at least, yields a significant contribution, values for D_{12} may be obtained with an accuracy similar to that of the determination of a under favorable conditions, i.e., of about 1 to 2%. An example for the simultaneous measurement of two diffusion modes is illustrated in Fig. 6 for an equimolar methane–ethane mixture in the near-critical region, where the slow mode D_1, commonly associated with mass diffusion, can be measured with a high accuracy, whereas the determination of the weak second mode D_2, ascribed to thermal diffusivity, can—within a reasonable measurement time—be performed only with large data scatter.

4.3. Dynamic Viscosity

The determination of viscosity from a bulk liquid differs from the measurement of the other two properties described above, as it requires the addition of spherical seed particles, the diffusion coefficient D_p of which is measured and related through the Stokes–Einstein relation, Eq. (2), to the dynamic viscosity η.

Thus, the key to successful viscosity measurements is the choice of suitable seed particles, preferably in a size range of about 20 to 500 nm and with a very narrow size distribution, where the size is best calibrated in liquids with a known viscosity [34, 35]. Silica particles with various surface modifications are suitable for many liquids, as they are chemically inert and form stable dispersions. With the investigation of particle diffusion the setup is normally modified in view of the large scattering cross sections and slow processes prevailing, typically resulting in the choice of large scattering angles, often employing a homodyne detection and the use of low-power lasers.

While uncertainties close to that of the determination of the other properties described above may be obtained for simple fluids [35], the use of the method is of particular interest in connection with a simultaneous determination of D_{12} and in the vicinity of the critical consolute point [36, 53].

4.4. Sound Velocity and Sound Attenuation

For the determination of these properties the Brillouin lines of the spectrum are probed, normally using a heterodyne technique, where the frequency of the local oscillator is adjusted by a local oscillator in a way so that the resulting frequency spacing to the relevant Brillouin line can conveniently be resolved with the correlator employed.

In this way the determination of sound velocity has become a standard task for DLS, employed for both reference fluids and various refrigerants and refrigerant mixtures over a wide range of temperature and pressure [20, 39, 49, 54] (see Fig. 7). A typical uncertainty of 0.5 % can be achieved for both the liquid and the vapor phases.

In contrast, the measurement of the sound attenuation D_s is subject to a much larger uncertainty, about 10 %, which is founded mainly in the lack

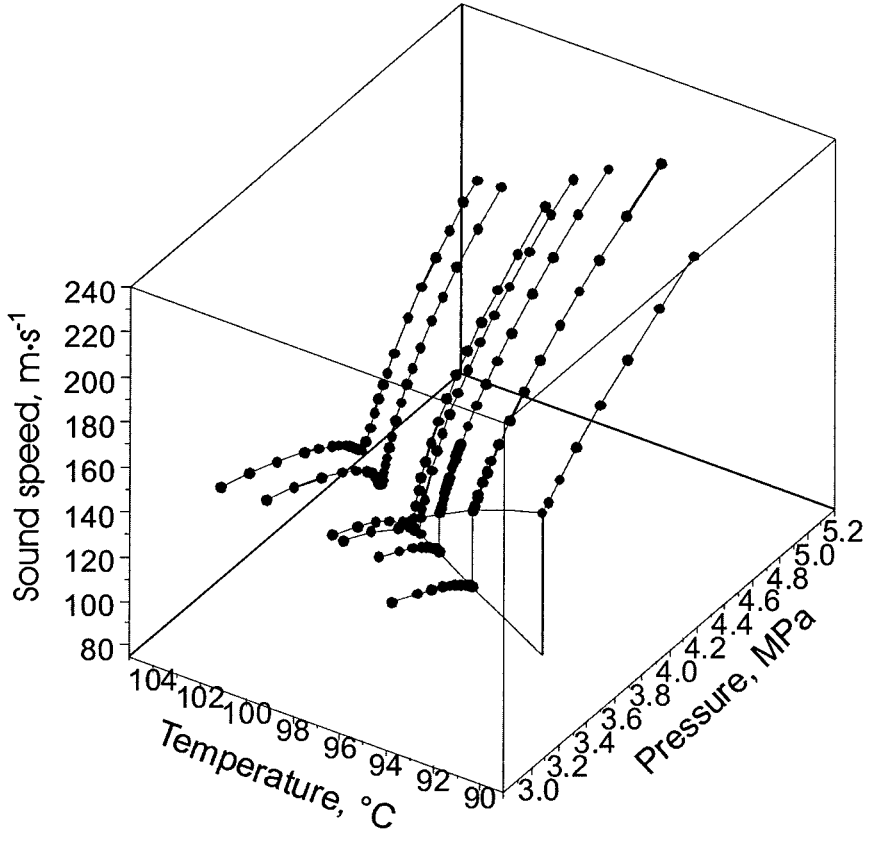

Fig. 7. Sound velocity of refrigerant R134a around the critical point [54].

of definition in the position of the Brillouin lines brought about by the fundamental small spread of scattering angles involved in a DLS experiment. Although this effect is clearly smaller in the time domain as with a direct observation of the spectrum, it is still difficult to provide appropriate corrections to obtain a high accuracy. Also, measurements of both sound velocity and sound attenuation may basically be affected by dispersion effects. While naturally no measurement technique whatsoever can perform measurements in the true thermodynamic $\omega = 0$ limit and a possible effect is negligible in the case of c_s for most fluids of interest, a marked effect has been observed for the sound attenuation, e.g., of refrigerants [20].

4.5. Viscosity and Surface Tension

As in many applications of DLS, the variant surface light scattering makes it possible to determine two properties simultaneously; in the case of SLS this measurement is performed without any extra effort and, with surface tension and viscosity, yields two quantities whose determination by most other means requires two completely different sets of experimental equipment. While commonly the kinematic viscosity v is regarded as the property directly accessible in SLS experiments, it should be stressed that this is true only with the simplifying neglect of gas phase properties. A more rigorous evaluation, specifically, e.g., when the vapor pressure of a pure substance is not negligible, requires the knowledge of density values anyway [cf. Eq. (6)], so that the provision of kinematic viscosity v or dynamic viscosity η is fully equivalent.

From its very beginning, where equipment constraints prevented experiments with a sufficient resolution [22], SLS has matured into a widely applied technique, with specific interest, e.g., in the investigation of monolayers [27], polymer solutions [55], or liquid crystals [56].

Generally, in light scattering experiments involving fluid interfaces the same precautions have to be taken as in conventional measurements of surface tension. These relate to possible effects of a differing surface temperature due to evaporative cooling, which naturally is not relevant if measurements are performed in true thermodynamic equilibrium, or of the influence of contamination and specifically of surfactants. With proper experimental care, however, no measurable differences between the values obtained by SLS and by conventional methods, in part relying on bulk properties, could be found [28, 57].

An uncertainty of down to 1% for either property can be obtained with SLS [28, 29] yet requires a proper execution of the method particularly as to the viscosity. This value is at least comparable with the uncertainty of conventional methods and, together with the great advantage

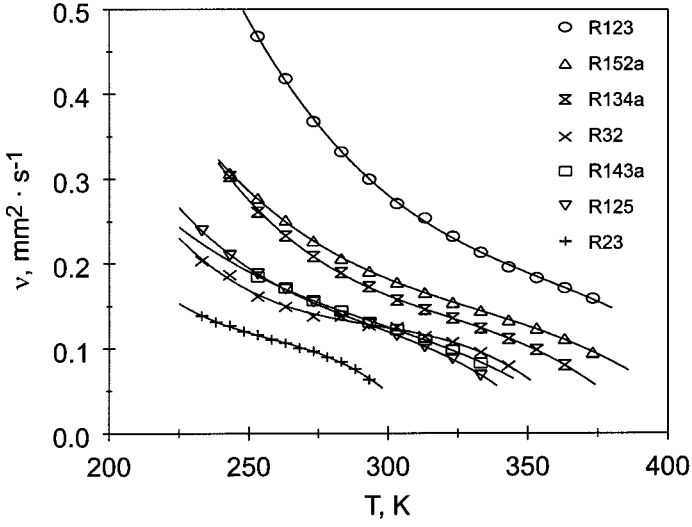

Fig. 8. Liquid viscosities v of refrigerants at saturation obtained by SLS. Drawn lines are best fits to third-order polynomials.

of a simultaneous determination of surface tension and viscosity, makes the method interesting also for a routine measurement of these properties of simple fluids and mixtures [28, 29, 49, 58]. An example for measurements on various refrigerants is given in Figs. 8 and 9. Also, apart from studying specific surface properties the contactless operation makes SLS ideally suited for the investigation of high-temperature melts [59, 60], yet presently with clear limitations in accuracy.

4.6. Further and Derivable Properties

Another quantity that directly follows from the spectrum of light scattered in bulk fluids is the Landau–Placzek ratio S, which is defined as the ratio of the intensities of the Rayleigh to Brillouin lines and related to the isobaric and isochoric specific heats, c_p and c_v, through $S = I_R/(2I_B) = (c_p - c_v)/c_v$. The Landau–Placzek ratio may be obtained from a series of measurements with defined variations of the signal of the local oscillator [61].

Though usually measured by the laser-induced thermal grating technique, the Soret coefficient S_T may also be obtained through DLS experiments when a steady temperature gradient is applied to a liquid [62].

As DLS provides a large variety of transport and other thermophysical properties, it is obvious that these values may—in combination with other

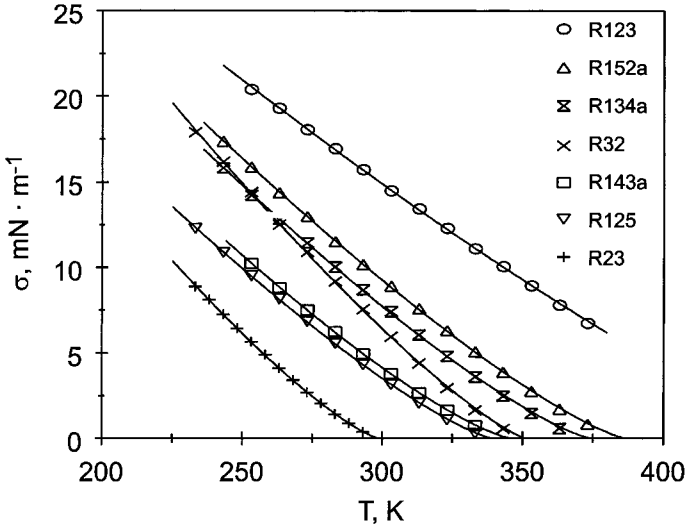

Fig. 9. Surface tensions σ of refrigerants at saturation obtained by SLS. Drawn lines are best fits based on van der Waals-type equations, $\sigma = \sigma_0(1 - T/T_c)^n$, where T_c is the critical temperature.

data—be used to derive still further thermophysical properties. The input parameters from DLS which may be regarded to be of particular importance in this context are the thermal diffusivity a, as it is not readily obtained by other techniques, and the sound velocity c_s, as it is of central importance for fundamental equations of state. A short survey on the derivation of other properties from DLS data has been given previously [10].

5. CONCLUSION

Through the—meanwhile—decades, dynamic light scattering has matured from a technique for the qualitative observation of fluid phenomena to a powerful tool for the accurate and versatile measurement of thermophysical properties. The persistent advantage of a contactless measurement in thermodynamic equilibrium has, over the years, been accompanied by the increasing number of properties that may reliably be determined by DLS techniques.

Thus, DLS currently is and will certainly remain an important element in the determination of thermophysical properties. Besides its utilization as a standard tool for routine provision of data, improvements may still be expected for even more accurate measurements and an increasing number

of applications with simultaneous or combined determination of properties. Other challenges for the future certainly comprise the continuous extension to particular regions of state, such as in the case of high-temperature melts, connected with efforts to achieve good accuracy also here, and improvements in experimental design including the provision of compact sensors which may find their way into in-process applications.

ACKNOWLEDGMENTS

The authors would like to thank the large number of scientists who have made much of the work described herein possible only through their active contribution, fruitful collaboration, and valuable advice. Special thanks are due to A. P. Fröba for recent contributions and inspiring discussions. Financial support, especially by the Deutsche Forschungsgemeinschaft, is also gratefully acknowledged.

REFERENCES

1. J. B. Armstrong, S. F. Y. Li, and W. A. Wakeham, *ASME Winter Annual Meeting 1982*, Paper 82-WAHT-84.
2. W. A. Wakeham, A. Nagashima, and J. V. Sengers (eds.), *Measurement of the Transport Properties of Fluids* (Blackwell Scientific, Oxford, 1991).
3. L. Onsager, *Phys. Rev.* **37**:405 (1931); **38**:2265 (1931).
4. B. J. Berne and R. Pecora, *Dynamic Light Scattering with Applications to Chemistry, Biology, and Physics* (Robert E. Krieger, Malabar, 1990).
5. B. Chu, *Laser Light Scattering: Basic Principle and Practice* (Academic, Boston, 1991).
6. W. Brown (ed.), *Dynamic Light Scattering—The Method and Some Applications* (Clarendon, Oxford, 1993).
7. A. Leipertz, *Int. J. Thermophys.* **9**:897 (1988).
8. J. N. Shaumeyer, R. W. Gammon, and J. V. Sengers, in Ref. 2, pp. 197–213.
9. K. Kraft, S. Will, and A. Leipertz, *Measurement* **14**:135 (1994).
10. A. Leipertz, *Fluid Phase Equil.* **125**:219 (1996).
11. Y. Nagasaka, T. Hatakeyma, M. Okuda, and Y. Nagashima, *Rev. Sci. Instr.* **59**:1156 (1988).
12. Y. Nagasaka, in Ref. 2, pp. 213–223.
13. T. J. Butenhoff, *Int. J. Thermophys.* **16**:1 (1995).
14. W. Köhler, C. Rosenauer, and P. Rossmanith, *Int. J. Thermophys.* **16**:11 (1995).
15. J. Wang and M. Fiebig, *Int. J. Thermophys.* **16**:1353 (1995).
16. R. D. Mountain, *Rev. Mod. Phys.* **38**:205 (1966); *J. Res. NBS* **70A**:207 (1966); *J. Res. NBS* **72A**:95 (1968).
17. A. Einstein, *Ann. Phys.* **17**:549 (1905); *Z. Elektrochem.* **17**:235 (1908).
18. Y. Yeh, *Appl. Opt.* **8**:3886 (1969).
19. G. Simonsohn, *Opt. Acta* **30**:875; 1675 (1983).
20. K. Kraft and A. Leipertz, *Int. J. Thermophys.* **16**:445 (1995).
21. W. Brouwer and R. K. Pathria, *Phys. Rev.* **163**:200 (1967).
22. R. H. Katyl and U. Ingard, *Phys. Rev. Lett.* **19**:64 (1967); **20**:68 (1968).

23. E. Mazur and D. S. Chung, *Physica A* **147**:387(1987).
24. D. Langewin (ed.), *Light Scattering by Liquid Surfaces and Complementary Techniques* (Marcel Dekker, New York 1992).
25. A. Hajiloo and J. C. Slattery, *J. Colloid Interface Sci.* **112**:325 (1986)
26. C. Earnshaw, *Appl. Opt.* **36**:7583 (1997).
27. D. McQueen and I. Lundström, *J. Chem. Soc. Faraday Trans. I* **69**:694 (1973).
28. A. P. Fröba and A. Leipertz, *Int. J. Thermophys.* **22**:41 (2001).
29. A. P. Fröba, S. Will, and A. Leipertz, *Int. J. Thermophys.* **21**:1225 (2000).
30. M. A. Bouchiat, in Ref. 24, pp. 35–59.
31. R. W. Gammon, H. L. Swinney, and H. Z. Cummins, *Phys. Rev. Lett.* **19**:1467 (1967).
32. P. Jany and J. Straub, *Int. J. Thermophys.* **8**:165 (1987).
33. S. Will and A. Leipertz, *Int. J. Thermophys.* **20**:791 (1999).
34. S. Will and A. Leipertz, *Int. J. Thermophys.* **16**:433 (1995).
35. S. Will and A. Leipertz, *Int. J. Thermophys.* **18**: 1339 (1997).
36. S. Will and A. Leipertz, in *Diffusion in Condensed Matter*, J. Kärger, P. Heitjans, and R. Haberlandt, eds. (Vieweg, Wiesbaden, 1999), pp. 219–244.
37. N. C. Ford, Jr., in *Dynamic Light Scattering*, R. Pecora, ed. (Plenum, New York, 1985), pp. 7–58.
38. S. Will and A. Leipertz, *Rev. Sci. Instr.* **67**:3164 (1996).
39. S. Will, A. Fröba, and A. Leipertz, *Int. J. Thermophys.* **19**:403 (1998).
40. J. Ricka, *Appl. Opt.* **32**: 2860 (1993).
41. K. Schätzel, *Quantum Opt.* **2**:287, 467 (1990).
42. S. Will and A. Leipertz, *Appl. Opt.* **32**:3813 (1993).
43. A. P. Fröba, S. Will, and A. Leipertz, *Appl. Opt.* **36**:7615 (1997).
44. K. Sakai, P. K. Choi, H. Tanaka, and K. Takagi, *Rev. Sci. Instr.* **62**:1192 (1996).
45. W. V. Meyer, J. A. Lock, H. M. Cheung, T. W. Taylor, P. Tin, and J. A. Mann, Jr., *Appl. Opt.* **36**:7605 (1997).
46. D. S. Chung, K. Y. Lee, and E. Mazur, *Appl. Phys. B* **64**:1 (1997).
47. B. Kruppa and J. Straub, *Exp. Therm. Fluid Sci.* **6**:28 (1993).
48. K. Kraft, M. Matos Lopes, and A. Leipertz, *Int. J. Thermophys.* **16**:423 (1995).
49. A. P. Fröba, S. Will, and A. Leipertz, submitted for publication.
50. G. Wu, M. Fiebig, and A. Leipertz, *Int. J. Heat Mass Transfer* **31**:1471, 2555 (1988).
51. B. J. Ackerson and H. J. M. Hanley, *J. Chem. Phys.* **73**:3568 (1980).
52. A. P. Fröba, S. Will, and A. Leipertz, *Int. J. Thermophys.* **21**:603 (2000).
53. H. Saad and E. Gulari, *J. Phys. Chem.* **88**:136 (1984).
54. K. Kraft and A. Leipertz, *DKV-Tagungsberichte* **22**:199 (1995).
55. Q. R. Huang and C. H. Wang, *J. Chem. Phys.* **109**:6103 (1999).
56. A. Böttger and J. G. H. Loosten, *Europhys. Lett.* **4**:1297 (1987).
57. S. Hård and R. D. Neuman, *J. Coll. Interface Sci.* **115**:73 (1987).
58. R. B. Dorshow and R. L. Swofford, *J. Appl. Phys.* **65**:3756 (1989).
59. T. Nishio and Y. Nagasaka, *Int. J. Thermophys.* **16**:1087 (1995).
60. M. Ohnishi and Y. Nagasaka, *High Temp.-High Press.* **32**:131 (2000).
61. G. Simonsohn and F. Wagner, *J. Phys. D* **24**:415 (1991).
62. W. B. Li, J. V. Sengers, R. W. Gammon, and P. N. Segré, *Int. J. Thermophys.* **16**:23 (1995).